Journal of Sound and Vibration 329 (2010) 394–414

Contents lists available at ScienceDirect

Journal of Sound and Vibration

journal homepage: www.elsevier.com/locate/jsvi

Velocity measurements in jets with application to noise source modeling

Philip J. Morris [a,*], K.B.M.Q. Zaman [b]

[a] Department of Aerospace Engineering, Penn State University, University Park, PA 16802, USA
[b] Inlet & Nozzle Branch, NASA Glenn Research Center, Cleveland, OH 44135, USA

ARTICLE INFO

Article history:
Received 7 February 2009
Received in revised form
16 September 2009
Accepted 18 September 2009
Handling Editor: P. Joseph
Available online 14 October 2009

ABSTRACT

This paper describes an experimental investigation of the statistical properties of turbulent velocity fluctuations in an axisymmetric jet. The focus is on those properties that are relevant to the prediction of noise. Measurements are performed using two single hot-wire anemometers as well as a two-component anemometer. Two-point cross correlations of the axial velocity fluctuations and of the fluctuations in the square of the axial velocity fluctuations are presented. Several reference locations in the jet are used including points on the jet lip and centerline. The scales of the turbulence and the convection velocity are determined, both in an overall sense as well as a function of frequency. The relationship between the second and fourth order correlations is developed and compared with the experimental data. The implications of the use of dimensional as well as non-dimensional correlations are considered. Finally, a comparison is made between the length scales deduced from the flow measurements and a RANS CFD calculation.

1. Introduction

Jet noise prediction methods based on either the Lighthill or Lilley–Goldstein acoustic analogy, or alternative approaches, depend on models of the statistical properties of the turbulence. These can be expressed either in terms of the cross correlation of the turbulent velocity fluctuations or its Fourier transform, the cross spectral density. There have only been a limited number of measurements of these properties in jets in the past: often only examining limited regions of the jet. These include the measurements by Davies et al. [1], Bradshaw et al. [2], Davies [3], and Chu [4]. Michalke and Fuchs [5] made both hot-wire and inflow pressure measurements. More recently, Harper-Bourne [6,7] revisited his earlier hot-wire anemometer measurements (1973) and provided additional cross correlation and cross coherence measurements as well as frequency-dependent convection velocities and length scales. These measurements, in particular those by Davies et al. [1] and Harper-Bourne [7], have been used to guide noise source modeling in jets. Noise predictions based on these models, such as those by Tam and Auriault [8] and Morris and Boluriaan [9], give good agreement with measurements, even though the flow measurements were made in much lower speed jets than those for which noise predictions were made. Recently, various optical velocity measurement techniques have been developed and used to determine the statistical properties of the jet turbulence. Bridges and Wernet [10], used particle image velocimetry (PIV) to measure space–time correlations in cold and heated jets with Mach numbers 0.5 and 0.9. Wernet [11] describes recent improvements in this technique with sampling rates up to 25 kHz. Kerhervé et al. [12] made two-point laser Doppler velocimeter (LDV) measurements in a cold

* Corresponding author.
E-mail address: pjm@psu.edu (P.J. Morris).

0022-460X/$ - see front matter © 2009 Elsevier Ltd. All rights reserved.
doi:10.1016/j.jsv.2009.09.024

Mach 1.2 jet. Since the LDV does not provide continuous time histories of the velocity, a "fuzzy-slotting" technique was used to construct the auto and cross correlations and the associated spectra. Kerhervé et al. [13] used the same two-point LDV technique to examine the frequency dependence of the turbulence length and time scales. Kerhervé and Fitzpatrick [14] extended these measurements and provided models for the variation of convection velocity and length scales with frequency. Chatellier and Fitzpatrick [15] used a combination of PIV and LDV to derive temporal correlation information from the low repetition rate PIV measurements. It should be noted that in these measurements the definition of the length scale was the traditional integral length scale used in turbulence studies and differs from the length scale definition used here and by Harper-Bourne [6,7], which is considered, by the present authors, to be more relevant to noise source modelling. Ukeiley et al. [16] used PIV to determine spatial correlations in a transonic jet. Correlations were determined with two orientations: one in the $x-r$ plane and the other in the $x-\theta$ plane. A dual PIV system was used by Fleury et al. [17] to make space–time correlations in unheated jets with Mach numbers 0.6 and 0.9. The temporal resolution of the correlations was restricted to fixed time separations. However, estimates of time as well as length scales were provided. Doty and McLaughlin [18] performed optical deflectometry (OD) measurements, a variant of schlieren visualization, in subsonic and supersonic jets. This technique provides continuous time histories of the density gradient fluctuations and was used to generate space–time correlations. Each of these techniques comes with experimental challenges; the need for seeding, the complexity of the data analysis, and the cost of the laser and optics. On the other hand the hot-wire anemometer is simple and cheap and, with careful use, can provide continuous time histories of velocity component fluctuations at multiple points in the jet flow. For the dimensions of the cross-wire probe used in the present experiments, the spatial resolution is comparable or better relative to PIV for a typical 12 in square field of view. PIV resolution improves if the area of the field of view is reduced. For boundary layer measurements, a single wire does better because the sensor diameter determines the spatial resolution (assuming 2-D flow). The biggest advantage of the hot-wire in measurement of the correlations is that it provides time-accurate data with high frequency response. This is not quite attainable yet with the other techniques. The drawbacks with the hot-wire anemometer are the possibility of probe interference effects, though efforts have been made to minimize them, and its restriction to low speed flows: the present measurements being made for a jet Mach number of 0.25. In addition, though it possesses high temporal resolution, the hot-wire anemometer only provides velocities at a single point.

The present paper aims to provide a more complete picture of the relevant turbulent statistics. This includes a wider range of reference points in the jet, the presentation of both cross spectra as well as cross correlations (including scales derived from these data), and the inclusion of both second as well as fourth order statistics. In addition, the validity of the quasi-normal hypothesis is examined. Finally, comparisons are made with a RANS prediction of the jet flow, both for the mean flow as well as the length scales, to determine how well such a simulation can provide estimates of scales for noise source modeling. The next section describes the experimental facility and methodology and the data analysis techniques. Key results are provided in Section 3. Finally, comparisons are made with results from a RANS simulation in Section 4 before providing a summary of the work in Section 5.

2. Experimental facility and data analysis

The data were obtained in an open jet facility at NASA Glenn Research Center. Compressed air supplied by a centrifugal blower entered through one end of a 0.762 m diameter cylindrical plenum chamber fitted with flow-conditioning units. The air discharged through a round, convergent nozzle at the other end of the chamber into the quiescent ambient of the test chamber. The nozzle had an exit diameter of 5.08 cm and all data were acquired for a nominal jet velocity of 87 m/s. The nozzle contours are shown in Fig. 1. The overall contraction ratio is 225. A trip ring was used to make the exit boundary layer turbulent. The trip ring was placed at $x=-4.45$ cm ($x/D_j=-0.876$) upstream of the jet exit where the nozzle interior radius was 1.418 cm ($r/D_j=0.558$). The ring was 0.318 cm wide and the downstream end had a thickness of 0.043 cm. A photograph of the nozzle, with the hot-wire probes placed near the exit, is shown in Fig. 2.

All data were acquired in 'cold' flow. That is, the jet was unheated and the total temperature everywhere was approximately the same as the ambient temperature. Two single miniature hot-film probes (TSI 1260A-10), together with a constant temperature anemometer (TSI IFA100), were used in the experiment. The active length of the single hot wire probes was 0.025 cm. The anemometer electronics were tuned to provide frequency response up to approximately 25 kHz. One probe was mounted on a 3-axis probe traversing mechanism operated under computer control. The second probe was mounted on a 2-axis manual traversing mechanism. The second probe was inserted in the flow at an angle and probe vibration and yield under the flow were kept to a minimum. For each run, the two probes were brought to within approximately 0.13 cm at the reference location. The computer controlled probe was then moved at different axial and radial locations for data acquisition. Limited measurements were also performed with a single X-wire probe (TSI 1248A-10) focusing on autocorrelations as described in Section 3.3. The active length of each of the cross hot-wire probes was also 0.025 cm.

2.1. Definitions

The results described in the following sections provide both second and fourth order two-point correlations of the axial velocity fluctuations in a jet. This section provides definitions of these correlations and the notation to be used in this paper.

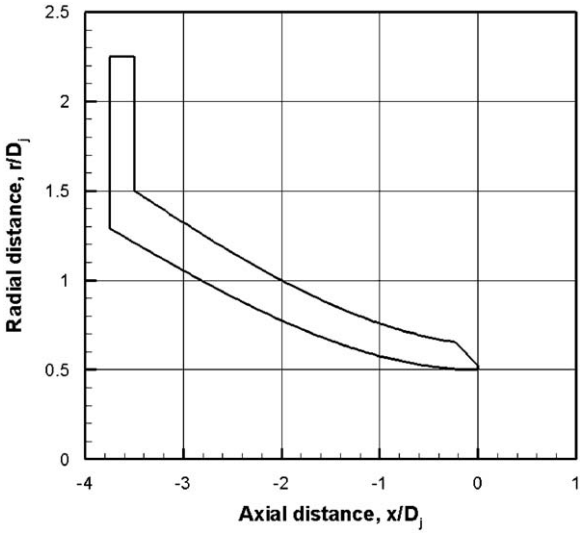

Fig. 1. Nozzle contours.

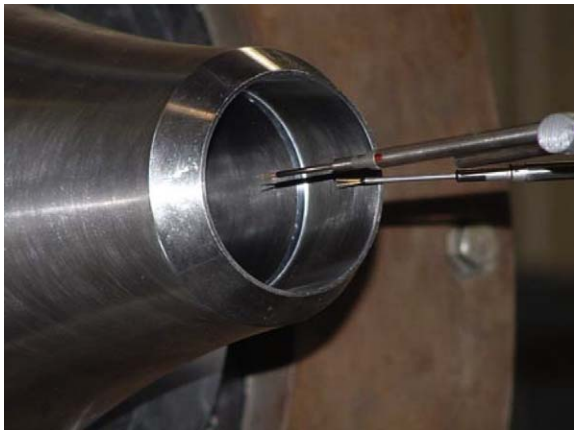

Fig. 2. Photograph of nozzle with two hot-wire probes placed near the exit. The trip ring inside the nozzle is visible.

Though axial velocity fluctuations constitute the majority of the measurements, the notation given here is generally applicable. The second order two-point correlation is defined by

$$R_{ij}(\mathbf{x},\boldsymbol{\eta},\tau)=\overline{u_i(\mathbf{x},t)u_j(\mathbf{x}+\boldsymbol{\eta},t+\tau)}, \tag{1}$$

where an overbar denotes time average, $u_i(\mathbf{x},t)$ is the velocity fluctuation in the i-th direction, and $\boldsymbol{\eta}$ and τ are the spatial separation and time delay, respectively. The correlation coefficient is obtained by dividing the cross correlation functions by the root mean square values of the velocity fluctuations at the two locations.

There are two choices for the fourth order cross correlation. These will be denoted by

$$R_{ijkl}(\mathbf{x},\boldsymbol{\eta},\tau)=\overline{u_iu_j(\mathbf{x},t)u_ku_l(\mathbf{x}+\boldsymbol{\eta},t+\tau)}, \tag{2}$$

and

$$C_{ijkl}(\mathbf{x},\boldsymbol{\eta},\tau)=\overline{(u_iu_j-\overline{u_iu_j})(\mathbf{x},t)(u_ku_l-\overline{u_ku_l})(\mathbf{x}+\boldsymbol{\eta},t+\tau)}. \tag{3}$$

The former correlation, Eq. (2), would be applicable to the equivalent source terms in Lilley's equation, as used, for example, by Khavaran and Bridges [19]. The latter cross correlation, Eq. (3), is relevant to the source description in Goldstein's [20] acoustic analogy, used recently by Karabasov et al. [21]. The corresponding cross correlation coefficients can be defined in a similar manner to the second order correlations. That is, in the first case, Eq. (2), the cross correlation coefficient is given by

$$r_{ijkl}(\mathbf{x},\boldsymbol{\eta},\tau)=\frac{R_{ijkl}(\mathbf{x},\boldsymbol{\eta},\tau)}{\sqrt{\overline{(u_iu_j)^2}(\mathbf{x})\overline{(u_ku_l)^2}(\mathbf{x}+\boldsymbol{\eta})}}. \tag{4}$$

In the second case, Eq. (3), it is given by

$$c_{ijkl}(\mathbf{x},\boldsymbol{\eta},\tau)=\frac{C_{ijkl}(\mathbf{x},\boldsymbol{\eta},\tau)}{\sqrt{\overline{(u_iu_j-\overline{u_iu_j})^2}(\mathbf{x})\overline{(u_ku_l-\overline{u_ku_l})^2}(\mathbf{x}+\boldsymbol{\eta})}}. \tag{5}$$

Alternatively, the correlation coefficient in the former case could be defined by normalizing with $R_{ijkl}(\mathbf{x},\mathbf{0},0)$.

At zero separation and time delay, and for $i=j=k=l=\alpha$, Eq. (4) reduces to

$$r_{\alpha\alpha\alpha\alpha}(\mathbf{x},\mathbf{0},0)=\overline{u_\alpha^4}(\mathbf{x})/[\overline{u_\alpha^2}(\mathbf{x})]^2, \tag{6}$$

where no summation is to be applied to α. This is the flatness factor for the u_α velocity fluctuation, which will be denoted by $T_\alpha(\mathbf{x})$. However, $c_{\alpha\alpha\alpha\alpha}(\mathbf{x},\mathbf{0},0)$ reduces to unity.

From Eqs. (2) and (3) it is readily shown that

$$C_{ijkl}(\mathbf{x},\boldsymbol{\eta},\tau)=R_{ijkl}(\mathbf{x},\boldsymbol{\eta},\tau)-\overline{u_iu_j}(\mathbf{x})\overline{u_ku_l}(\mathbf{x}+\boldsymbol{\eta}). \tag{7}$$

Also, at any location

$$\overline{(u_\alpha^2-\overline{u_\alpha^2})^2}=(\overline{u_\alpha^2})^2(T_\alpha-1). \tag{8}$$

So that, from Eqs. (5) and (6),

$$c_{\alpha\alpha\alpha\alpha}(\mathbf{x},\boldsymbol{\eta},\tau)=\frac{r_{\alpha\alpha\alpha\alpha}(\mathbf{x},\boldsymbol{\eta},\tau)-1}{\sqrt{[T_\alpha(\mathbf{x})-1][T_\alpha(\mathbf{x}+\boldsymbol{\eta})-1]}}. \tag{9}$$

In noise source modeling, the quasi-normal hypothesis [22] is often used to relate the fourth and second order correlations. In the general case, the hypothesis is given by

$$R_{ijkl}=R_{ik}R_{jl}+R_{il}R_{jk}+R_{ij}R_{kl}. \tag{10}$$

Clearly this gives $T_\alpha(\mathbf{x})=3$. However, Lighthill [23] showed that, if the mean square turbulent velocity fluctuations and the flatness factor are independent of the separation distance, then

$$c_{\alpha\alpha\alpha\alpha}(\mathbf{x},\boldsymbol{\eta},\tau)=r_{\alpha\alpha}^2(\mathbf{x},\boldsymbol{\eta},\tau). \tag{11}$$

This holds for all values of flatness factor (as long as the mean square velocity fluctuations and flatness factor are independent of $\boldsymbol{\eta}$). When the quasi-normal hypothesis is not applied, Eqs. (9) and (11) give

$$r_{\alpha\alpha\alpha\alpha}=1+(T_\alpha(\mathbf{x})-1)r_{\alpha\alpha}^2. \tag{12}$$

Thus, unless the quasi-normal hypothesis is used, the source term correlations require knowledge of the flatness factor. It should also be noted that the analysis given by Lighthill [23] is for correlations between velocity fluctuations in the same direction. However, it appears that this result can be extended, though the resulting expressions are more complicated.

The cross spectral densities are given by the Fourier transform of the cross correlations with respect to time delay. That is, for example,

$$S_{ijkl}(\mathbf{x},\boldsymbol{\eta},\omega)=\frac{1}{2\pi}\int_{-\infty}^{\infty}C_{ijkl}(\mathbf{x},\boldsymbol{\eta},\tau)\mathrm{e}^{-\mathrm{i}\omega\tau}\,\mathrm{d}\tau, \tag{13}$$

with

$$C_{ijkl}(\mathbf{x},\boldsymbol{\eta},\tau)=\int_{-\infty}^{\infty}S_{ijkl}(\mathbf{x},\boldsymbol{\eta},\omega)\mathrm{e}^{\mathrm{i}\omega\tau}\,\mathrm{d}\omega, \tag{14}$$

where ω is the radian frequency. In addition, a complex cross coherence can be defined by

$$s_{ijkl}(\mathbf{x},\boldsymbol{\eta},\omega)=\frac{S_{ijkl}(\mathbf{x},\boldsymbol{\eta},\omega)}{\sqrt{S_{ijkl}^2(\mathbf{x},\omega)S_{ijkl}^2(\mathbf{x}+\boldsymbol{\eta},\omega)}}, \tag{15}$$

where the terms in the numerator represent the auto-spectra at $\mathbf{x}$ and $\mathbf{x}+\boldsymbol{\eta}$. The magnitude of $s_{ijkl}(\mathbf{x},\boldsymbol{\eta},\omega)$ is the square root of the coherence. Similar expressions can be derived for the second order cross spectral density. Similar definitions of the complex cross coherence were given by Kerhervé et al. [13].

2.2. Data analysis

The hot-wire signals were sampled at 35 kHz and, for the correlation results presented in this paper, 10 s of data were acquired at each point. The signals were first converted to velocity using a calibration obtained in the core of the jet and a fourth-order polynomial fit to the velocity–voltage relationship. The time series for the velocity were divided into 50 percent overlapping segments. Typically, each segment consisted of 1024 samples, though other longer sample lengths gave very similar results. This gave 681 overlapping segments. A Hanning window was applied to each segment, its fast Fourier transform was taken, and the transforms were averaged. The auto and cross spectra were then obtained by taking the product of the averaged transforms with their complex conjugates. An inverse fast Fourier transform was then used to

obtain the auto and cross correlations and their coefficients. The amplitude and phase of the complex cross coherence was also calculated.

3. Experimental results

3.1. Single wire measurements

The mean velocity profiles were measured with the probe mounted on the 3-axis traversing mechanism. Fig. 3 shows boundary layer profiles measured near the exit of the nozzle. Integration of the mean velocity data provided the boundary layer characteristics. These data are presented in Table 1 compared to the properties for the untripped case. Fig. 4 shows the centerline variations of the axial mean velocity and turbulence intensity. It can be seen that the potential core length is approximately five jet diameters and the peak turbulence intensity reaches approximately 14 percent at approximately 9 diameters downstream of the jet exit. Note that the velocity relaxes to a slightly higher value just downstream of the exit. This is because the flow-lines are not yet parallel at the exit and the nozzle walls terminate with approximately a 0.15° convergence angle. The jet exit velocity is taken to be the maximum value, just downstream of the physical jet exit. It is also noted, with radial surveys at $x/D_j = 12$, that the geometric axis of the nozzle and the flow axis are aligned within 0.5°.

Radial surveys of the axial velocity were made at axial locations between the jet exit and 10 jet diameters. Fig. 5 shows the mean axial velocity at several downstream locations. A similarity coordinate is used based on the axial mean half velocity point and the local vorticity thickness. That is,

$$\eta = (r - r_{0.5})/\delta_\omega, \tag{16}$$

with

$$\delta_\omega = U_j/\max|\partial\overline{u}/\partial r|. \tag{17}$$

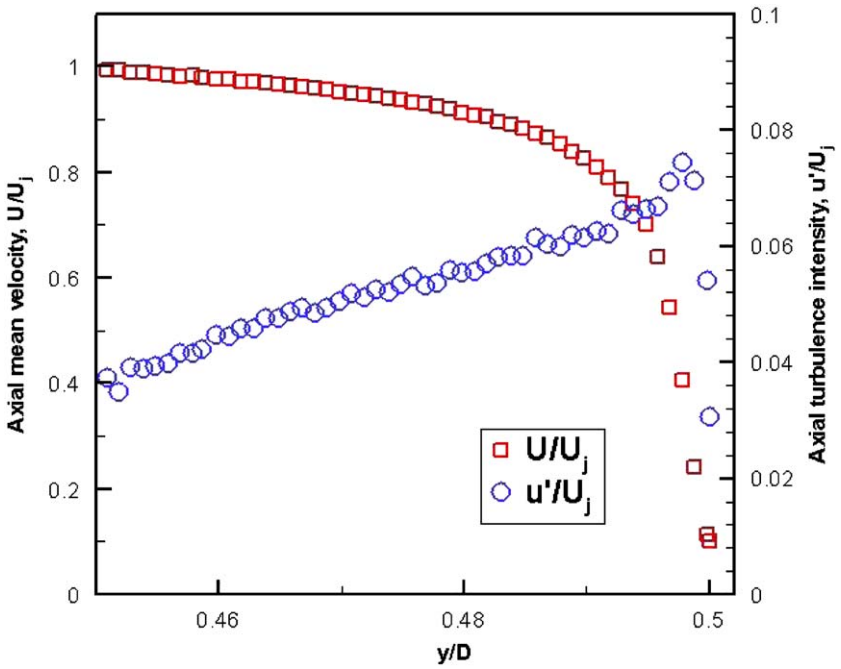

Fig. 3. Boundary layer profiles, measured about 0.05 cm downstream from the nozzle lip.

Table 1
Exit boundary layer displacement thickness δ_1, momentum thickness δ_2, shape factor H_{12}, and peak turbulence intensity for the tripped and untripped cases.

	Untripped	Tripped
δ_1 (cm)	0.0076	0.0135
δ_2 (cm)	0.0033	0.0097
$H_{12} = \delta_1/\delta_2$	2.33	1.39
Peak turbulence intensity	0.067	0.075

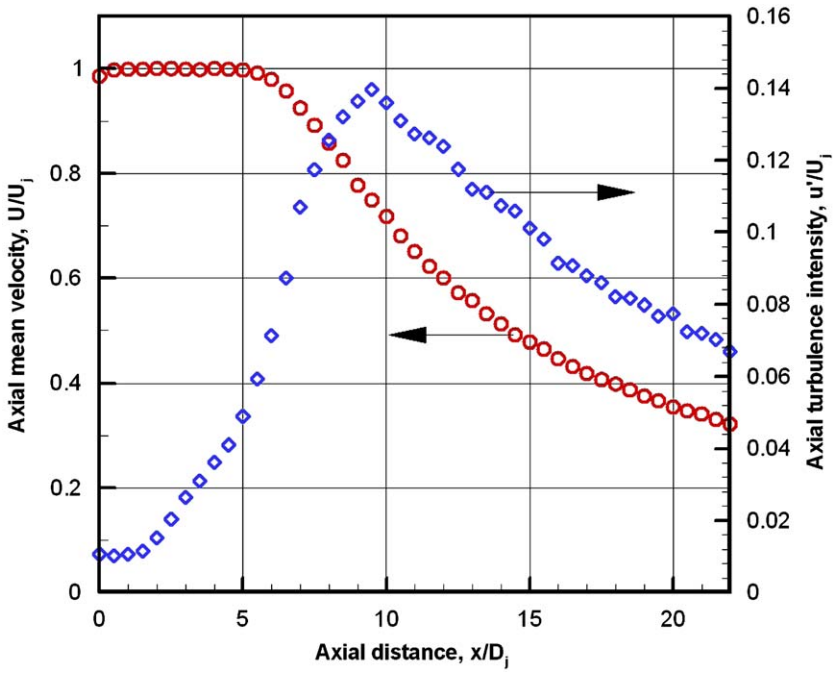

Fig. 4. Centerline variations of axial mean velocity and turbulence intensity.

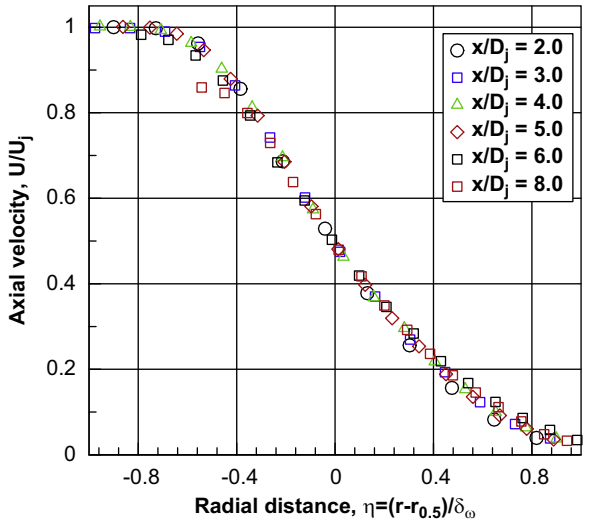

Fig. 5. Radial variation of the axial mean velocity.

Even though the final two axial locations are downstream of the end of the potential core, the use of the jet exit velocity in the definition of the vorticity thickness, rather than the jet centerline velocity, provides an improved collapse of the data. This reflects the persistence of the similarity properties of the annular jet mixing region downstream of the end of the jet potential core. There is some deviation close to the jet centerline at the last two axial locations, which is to be expected. The corresponding axial turbulence intensities are shown in Fig. 6. It is clear that the jet turbulence behaves in a self-similar manner over this entire region.

3.2. Two wire measurements

In this section, initially, results will be given in some detail for the region near the end of the potential core: both on the jet lip line and on the jet centerline. It can be seen from Fig. 4 that, at $x/D_j = 5$ the turbulence intensity on the jet centerline

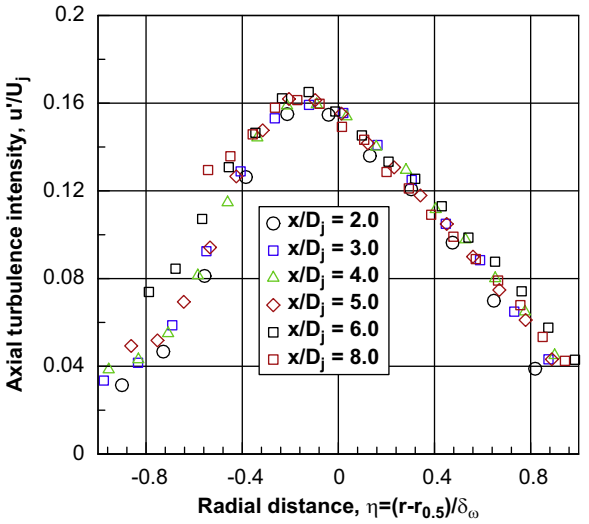

Fig. 6. Radial variation of the axial turbulence intensity.

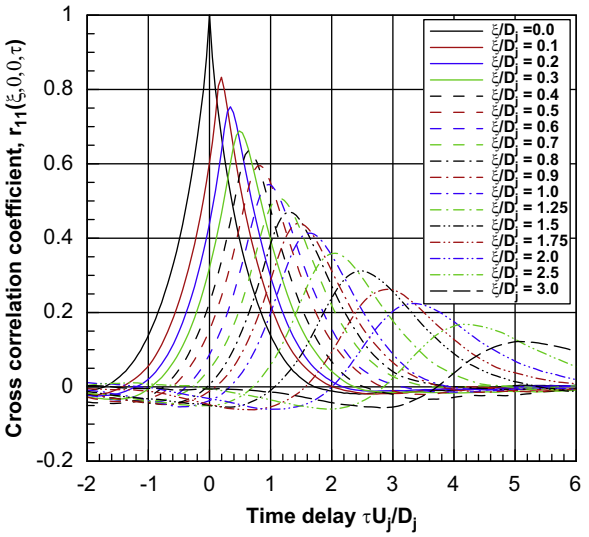

Fig. 7. Second order cross correlation coefficient: $x/D_j = 5$ and $r/D_j = 0.5$.

has not yet reached its maximum value. However, as shown in Fig. 6, the turbulence intensity on the jet lip line is almost constant at its maximum value.

3.2.1. Lip line measurements

In the results in this section, the second and fourth order correlations and correlation coefficients are defined by Eqs. (1), (3) and (5). Figs. 7 and 8 show the second and fourth order axial cross correlation coefficients. Note that the dependence of the correlations on **x** is implied, and the arguments refer to (ξ, η, ζ, τ), where the separation distance $\boldsymbol{\eta} = (\xi, \eta, \zeta)$. The fourth order cross correlation decays more rapidly, both in separation distance and time delay. It should also be noted that, for larger separations, the second order cross correlations show noticeable negative loops. This is consistent with a view of the turbulence that it consists of two components: a first that is relatively poorly correlated, both spatially and temporally, and a second that is more coherent and has a wavelike character. If the points of maximum cross correlation are determined as a function of separation distance, the overall convection velocity of the turbulence can be estimated. This is shown in Fig. 9. The convection speed for the velocity fluctuations is given by $u_c/U_j = 0.623$ and that for the square of the velocity fluctuations is $u_c/U_j = 0.655$. It should be noted that the resolution for the time delay is given by $\Delta\tau = 0.0489$. Also, the linear fits to the measurements do not pass through the origin. This indicates that the initial probe separation, which was set by eye, was not exact. The estimated axial positioning error is approximately 0.05 cm.

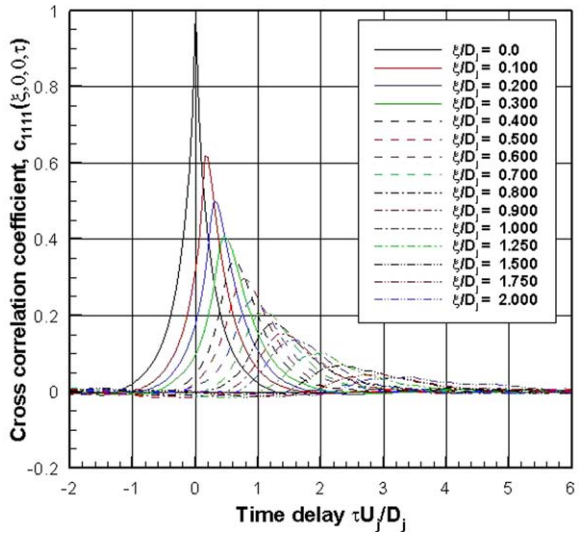

Fig. 8. Fourth order cross correlation coefficient: $x/D_j = 5$ and $r/D_j = 0.5$.

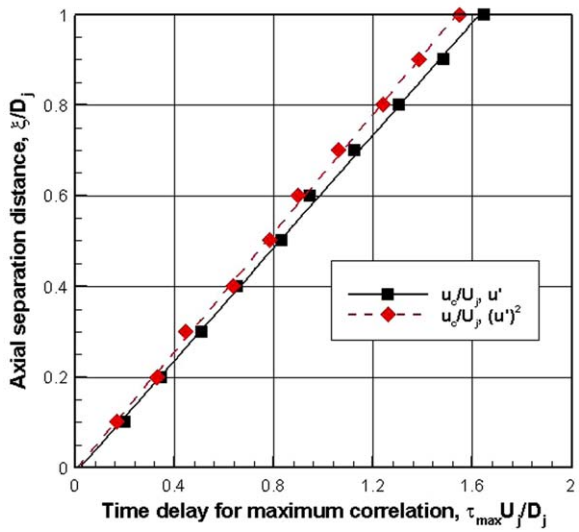

Fig. 9. Variation of time delay for maximum cross correlation with separation distance for the second and fourth order cross correlation coefficients: $x/D_j = 5$ and $r/D_j = 0.5$.

The second and fourth order spatial correlation coefficients are shown in Fig. 10. Also shown is the fourth order spatial correlation based on Eq. (11). The agreement is very good. It should be noted that the fourth order cross correlation does have very small negative loops, which are clearly not possible using Eq. (11). However, the magnitude of these loops is likely to be of the order of accuracy of the measurements and data analysis. Also, at this location, the flatness factor, $T_1 = 2.56$.

Fisher and Davies [24], Davies [3] and Harper-Bourne [7] used analog filtering to obtain the cross spectral properties. In the present study, and that by Kerhervé et al. [13], the cross spectral density and its associated properties are obtained digitally. This reduces some of the issues associated with the analog filter bandwidth and shape. Fig. 11 shows the phase of the complex cross coherence, defined in Eq. (15), as a function of axial separation distance. The phase for both the second and fourth order cases are shown as they are very similar. If the variation of the phase of the cross spectral density (or complex cross coherence) is determined as a function of the separation distance, then the frequency variation of the phase velocity is given by

$$u_c(St) = 2\pi St/|\mathrm{d}\varphi/\mathrm{d}\xi|. \tag{18}$$

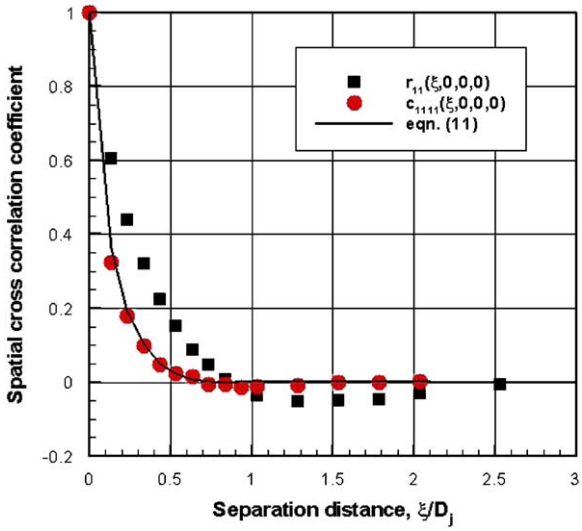

Fig. 10. Second and fourth order spatial cross correlations and fourth order cross correlation calculated using Eq. (11): $x/D_j = 5$ and $r/D_j = 0.5$.

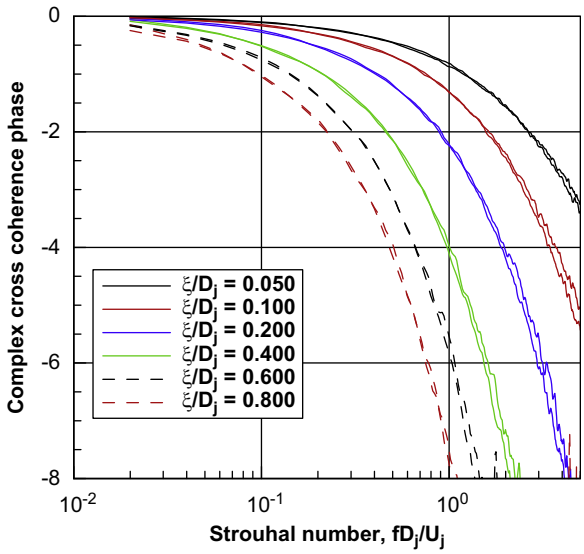

Fig. 11. Variation of the phase of the complex cross coherence with separation distance. Both second and fourth order phase variations are shown: $x/D_j = 5$ and $r/D_j = 0.5$.

Fig. 12 shows the variation of the phase velocity as a function of Strouhal number. Only the results for the fourth order case are shown. Also, shown is a power law fit to the data. It is given by,

$$u_c/U_j(St) = 0.062\ln(St) + 0.701. \tag{19}$$

This is in very good agreement with the curve fit given by Harper-Bourne [7] who found coefficients, 0.056 and 0.667.

Figs. 13 and 14 show the variation of the amplitude of the complex cross coherence as a function of separation distance for the second and fourth order correlations, respectively. In this case there are some differences. For the second order cross coherence the decay with separation distance is much slower for Strouhal numbers of in the region of $St = 0.2$. This is consistent with the cross correlations shown in Fig. 7 and provides further evidence of a coherent component of the turbulence in this frequency range. The turbulence axial length scale can be estimated by determining the variation of coherence amplitude with separation distance. In the present experiments the length scale is set to the $1/e$ decay point in the decay of the amplitude of the cross coherence. For the majority of the locations in the jet an exponential function is a good representation of the cross coherence amplitude variation with separation distance. It should be emphasized that this definition, introduced by Harper-Bourne [6] is not the traditional integral length scale, such as that used by Kerhervé et al. [13]. However, it does represent the decay length scale that has been used extensively in modeling the two-point turbulent

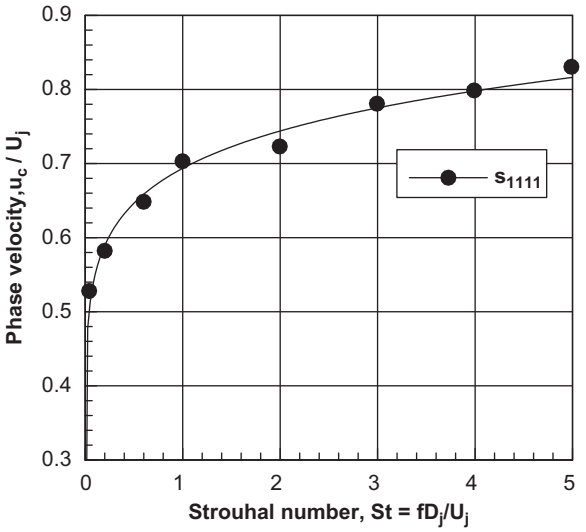

Fig. 12. Variation of phase velocity with Strouhal number for fourth order complex cross coherence: $x/D_j = 5$ and $r/D_j = 0.5$.

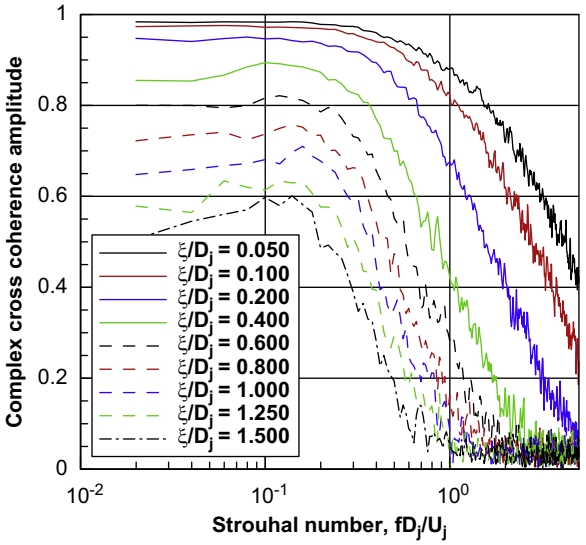

Fig. 13. Amplitude of second order complex cross coherence as a function of axial separation distance: $x/D_j = 5$ and $r/D_j = 0.5$.

statistics in jets for noise modeling purposes. It avoids the difficulties that might occur if significant negative loops occur in the cross correlations. These could cause the integral length scale to be zero. The variation of the axial, radial and azimuthal length scales with Strouhal number is shown in Fig. 15. The length scales are again defined by the $1/e$ point in the decay of the cross coherence. The radial and azimuthal length scales were obtained the same manner as the axial length scales, based on the displacement of the movable probe in the radial and azimuthal directions. The length scale for the second order correlation is greater than that for the fourth order in all directions. At low Strouhal numbers the length scales are almost constant, with a slight increase at approximately $St = 0.2$. At high Strouhal numbers the length scales decay inversely with Strouhal number. This is consistent with suggestion by Morris and Boluriaan [9] and Self [25]. In the former case, the length scale was taken to be

$$L/D_j = [1 - \exp(-c_s StL/D_j)]/(c_s St). \tag{20}$$

Then, at high Strouhal numbers the length scale is inversely proportional to Strouhal number, whereas at lower Strouhal numbers the length scale is independent of Strouhal number. The axial length scales, based on the $1/e$ values for the spatial correlations, shown in Fig. 10 are $0.295D_j$ and $0.126D_j$ for the second and fourth order correlations, respectively. These are much smaller than the length scales at lower Strouhal numbers shown in Fig. 15. This suggests that the initial decay of the spatial cross correlation is dominated by the high frequency or shorter wavelength disturbances.

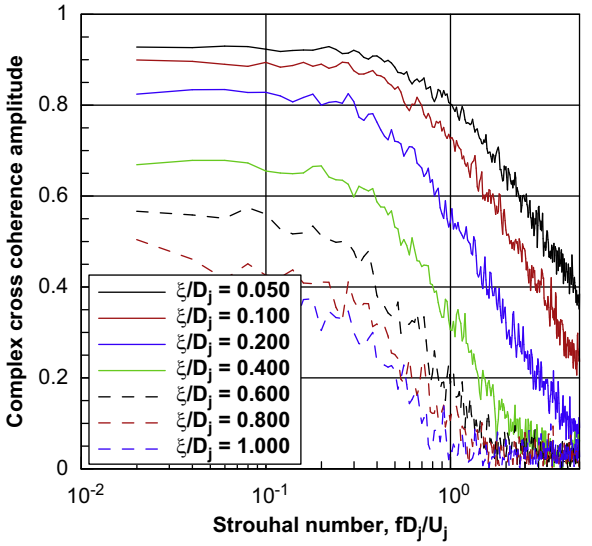

Fig. 14. Amplitude of fourth order complex cross coherence as a function of axial separation distance: $x/D_j = 5$ and $r/D_j = 0.5$.

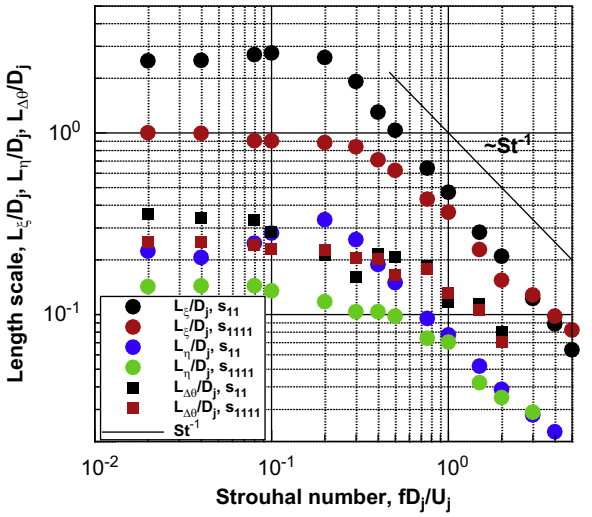

Fig. 15. Variation of axial, radial and azimuthal length scales with Strouhal number: $x/D_j = 5$ and $r/D_j = 0.5$.

The measurements at $x/D_j = 9$, $r/D_j = 0.5$ show very similar trends to the measurements at $x/D_j = 5$, $r/D_j = 0.5$. The overall convection velocity is measured to be $0.56U_j$ for the velocity fluctuations and $0.614U_j$ for the fluctuation in the square of the velocity fluctuations. The local mean axial velocity equals $0.54U_j$. The maximum turbulence intensity at this axial location occurs slightly inside the jet lip line, where the local mean velocity equals $0.6U_j$. The spatial cross correlations are shown Fig. 16, for both the second and fourth order correlations. The length scales are $0.295D_j$ and $0.126D_j$ for the second and fourth order correlations, respectively. The estimate of the fourth order spatial cross correlation using Eq. (11) is also shown. The agreement is good. If Eq. (11) were exact, then the ratio of the length scales would be exactly 2. The variation of the axial length scale with Strouhal number is shown in Fig. 17. The axial length scales at the lower Strouhal numbers are again almost constant and at high frequencies the length scales decay inversely with Strouhal number. A comparison with Fig. 15 shows that the length scales have increased at low Strouhal numbers, but are nearly unchanged at high Strouhal numbers. This suggests that the length scale of the lower Strouhal number disturbances scales with the physical width of the jet, whereas the small scale structures have a universal behavior, with a local Strouhal number based on length scale and velocity fluctuation that is independent of location in the jet.

3.2.2. Radial traverses

Before considering the behavior on the jet centerline, the radial variation of properties at $x/D_j = 5$ will be considered. Fig. 18 shows the variation of the convection velocity, based on the cross correlation coefficients as a function of radial

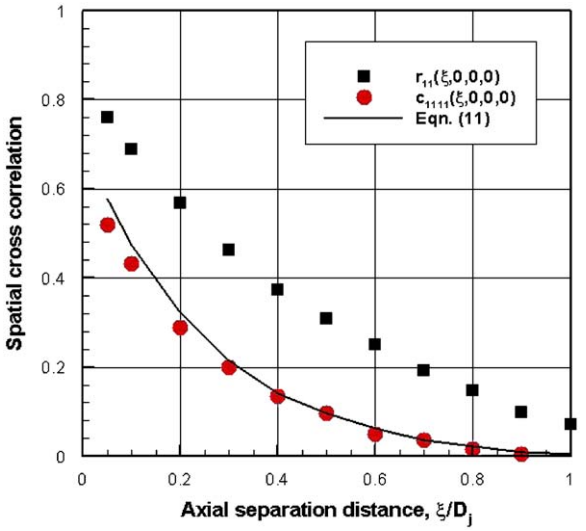

Fig. 16. Spatial cross correlation coefficients: $x/D_j = 9$ and $r/D_j = 0.5$.

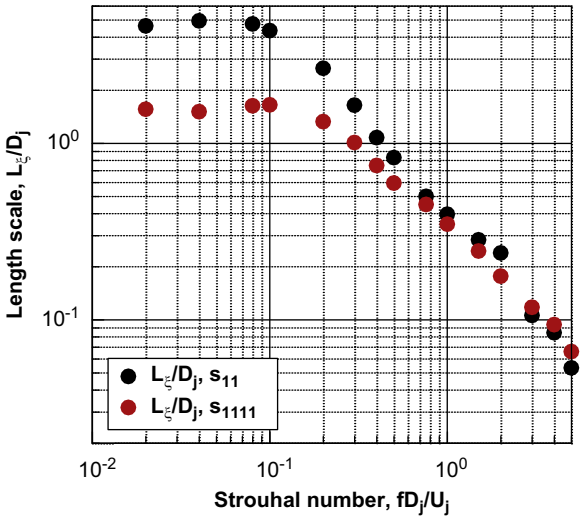

Fig. 17. Variation of axial length scales with Strouhal number: $x/D_j = 9$ and $r/D_j = 0.5$.

location. Inside the lip line, the convection velocity is less than the axial jet velocity, reaching a maximum value of $0.85U_j$ on the jet centerline. At the jet lip line, the convection velocity and jet axial velocity are almost equal with a value of $0.6U_j$. Thus, when estimating the convection velocity in noise source modeling, the use of the local axial mean velocity is a good approximation, as the lip line is the location of maximum velocity fluctuations. Outside the jet lip line, the convection velocity is higher than the local axial velocity. These results are consistent with earlier measurements: for example by Davies [3].

Another factor that is important in characterizing the relationship between the second and fourth order statistics is the flatness factor. The radial variation of the flatness factor at $x/D_j = 5$ is shown in Fig. 19. Also shown are measurements by Davies [3] at similar axial locations in a low speed jet. Note that the radial coordinate is given by $(r - D_j/2)/x$, to agree with the scale used by Davies. Near the jet lip line the flatness factor is slightly <3, the value for a normally distributed variable. At locations inside and outside the jet lip line the flatness factor rises to values of approximately 6 on the jet centerline. Thus, the use of a quasi-normal hypothesis in the region of maximum velocity fluctuations, near the jet lip line, is again reasonably well justified.

3.2.3. *Centerline measurements*

From Fig. 4 it can be seen that the centerline mean velocity begins to decay at approximately $x/D_j = 5$ and the maximum axial turbulence intensity occurs at approximately $x/D_j = 9$. In this section, measurements are described on the centerline

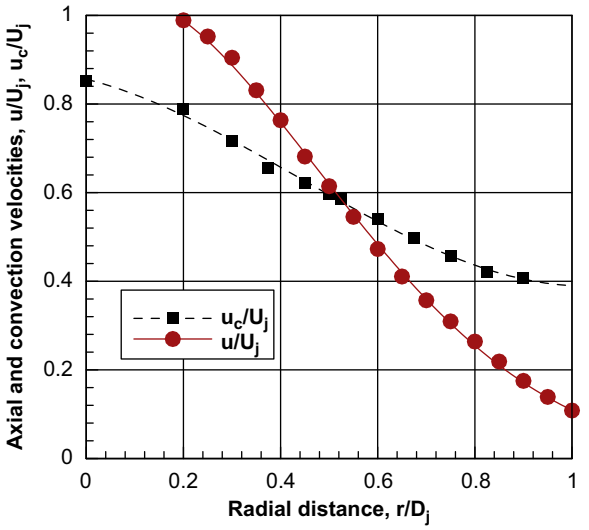

Fig. 18. Radial variation of the axial convection velocity: $x/D_j = 5$.

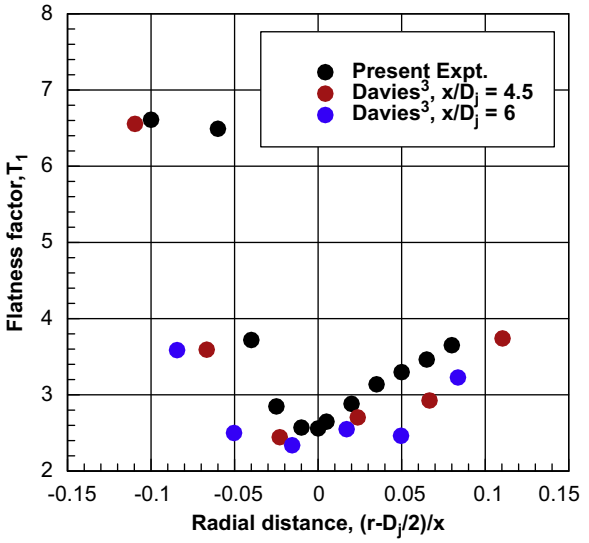

Fig. 19. Radial variation of flatness factor: T_1, $x/D_j = 5$.

at these axial locations. The second and fourth order axial cross correlation coefficients for the axial velocity are shown in Figs. 20 and 21, respectively. Measurements were made at additional intermediate axial separations, as well as at larger axial separations, but these are not shown for clarity. A noticeable feature is that an extrapolation of the peaks in the cross correlations does not quite reach the expected value of unity at $\tau = 0$. Even though efforts were made to minimize the probe interference, it is thought that the observed anomaly is likely due to such an effect. At x/Dj = 5 on the centerline the turbulence levels were low and, thus, the wake from the reference had a non-negligible effect on the downstream probe signal. This reduced the correlation amplitudes, especially at small separation distances. For the lip-line measurements, on the other hand, the interference was negligible as the turbulence levels were already high. It is also noticed that the negative loops in the second order cross correlations. These are strongly indicative of an average structure associated with traveling waves or large scale coherent structures. The corresponding power spectral density is shown in Fig. 22. There is a strong peak at approximately $St = 0.4$. This corresponds to the period of the oscillations evident in the cross correlations.

The second and fourth order spatial cross correlations are shown in Fig. 23. The agreement between the estimate of the fourth order statistics from Eq. (11) and the measurements is good. This is in spite of the fact that the flatness factor is approximately $T_1 = 7$ over the axial range of the measurements. The variation of the flatness factor with axial location for different radial locations is shown in Fig. 24. The maximum value of flatness factor occurs at approximately $x/D_j = 6$. The value of flatness factor on the centerline then falls rapidly. It equals the value at all other radial locations downstream of

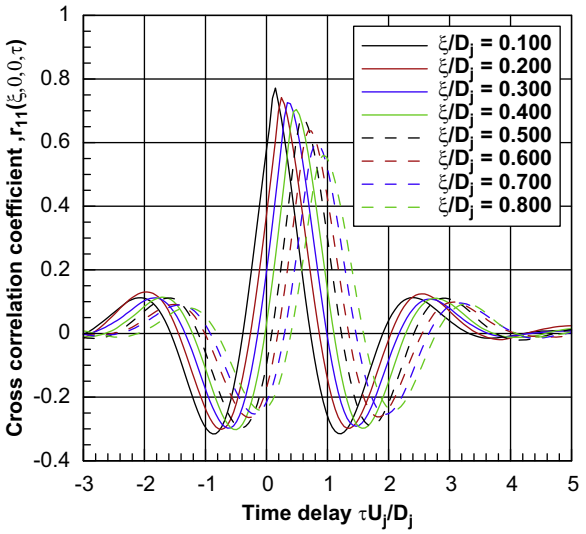

Fig. 20. Second order cross correlation coefficient: $x/D_j = 5$ and $r/D_j = 0.0$.

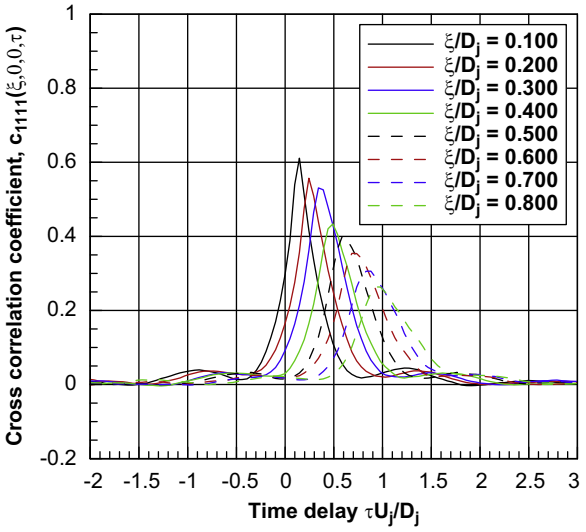

Fig. 21. Fourth order cross correlation coefficient: $x/D_j = 5$ and $r/D_j = 0.0$.

approximately $x/D_j = 9$. The values of the flatness factor at other radial locations follow a similar trend. It should be emphasized that if the fourth order statistics were estimated on the basis of the quasi-normal approximation at this location in the jet, then significant errors would occur. However the levels of the velocity fluctuations at this location are relatively low. So the error incurred in making this approximation would not be expected to have a noticeable effect on a radiated noise prediction.

The variation of the length scales with Strouhal number is shown in Fig. 25. The length scale based on the velocity fluctuation reaches a maximum at $St = 0.4$. This is the Strouhal number for the maximum in the power spectral density. It should be remembered that this length scale is based on the $1/e$ point for the amplitude of the complex cross coherence and can't be used to estimate the wavelength of the periodic structures that are dominating the spatial cross correlation.

For completeness, the axial length scales based on the overall spatial cross correlations, again using the $1/e$ value, are $0.159D_j$ and $0.123D_j$ for the second and fourth order correlations, respectively. The corresponding convection velocities are $0.88U_j$ and $0.83U_j$. The local axial mean velocity is equal to the jet exit velocity.

At this location on the jet centerline the turbulence intensity is changing rapidly, so the absolute value of the cross correlation decreases much more slowly than the cross correlation coefficient. This is shown in Fig. 26 for the second order cross correlation. It is clear that scales estimated on the basis of the dimensional cross correlation function would be much greater than those based on the cross correlation coefficient. However, it is the dimensional cross correlation of the source

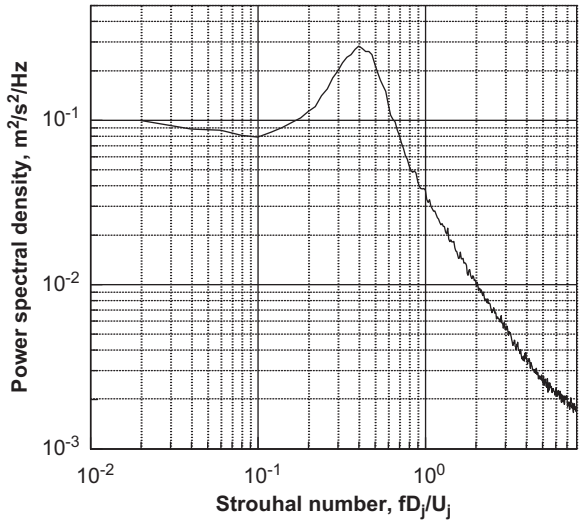

Fig. 22. Dimensional power spectral density of the axial velocity fluctuations: $x/D_j = 5$ and $r/D_j = 0.0$.

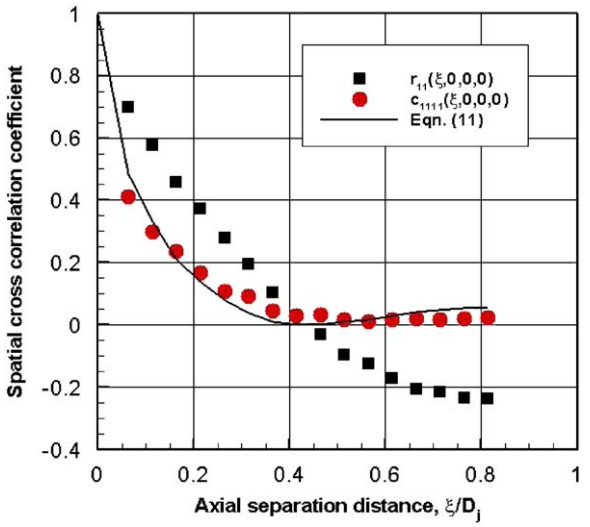

Fig. 23. Spatial cross correlation coefficients: $x/D_j = 5$ and $r/D_j = 0.0$.

statistics that is needed in the noise models. To minimize this potential problem, the use of a central reference location with both upstream and downstream separations should be used in the source modeling.

The final location to be considered is on the jet centerline at the location of the maximum axial turbulence intensity: $x/D_j = 9$, $r/D_j = 0.0$. The behavior at this location is very similar to that on the lip line at this axial location. For example the spatial cross correlation functions are shown in Fig. 27 and the variation of the axial length scales with Strouhal number is shown in Fig. 28. The axial length scales based on the spatial correlations are $0.341D_j$ and $0.154D_j$ for the second and fourth order correlations, respectively. The corresponding convection velocities are $0.70U_j$ and $0.65U_j$. The local mean axial velocity at this location is $0.80U_j$.

3.3. Cross wire measurements

The measurements have been limited to a single cross wire to avoid interference problems with the second probe. The primary use of the cross wire measurements here is the estimation of the second and fourth order autocorrelation magnitudes. In the noise source modeling described by Karabasov et al. [21], these values were obtained from large eddy simulations. Table 2 presents the values of the fourth order autocorrelations relative to C_{1111}. The values are lower than those given by Karabasov et al. [21], though there is considerable variation with position in the jet. In fact, perhaps

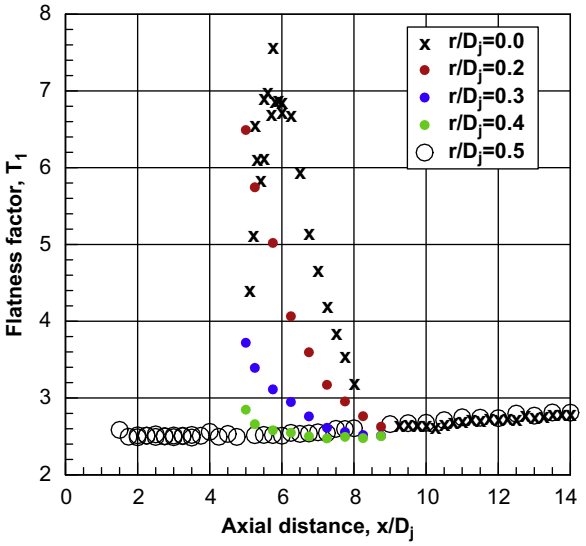

Fig. 24. Axial variation of flatness factor of axial velocity fluctuations at different radial locations.

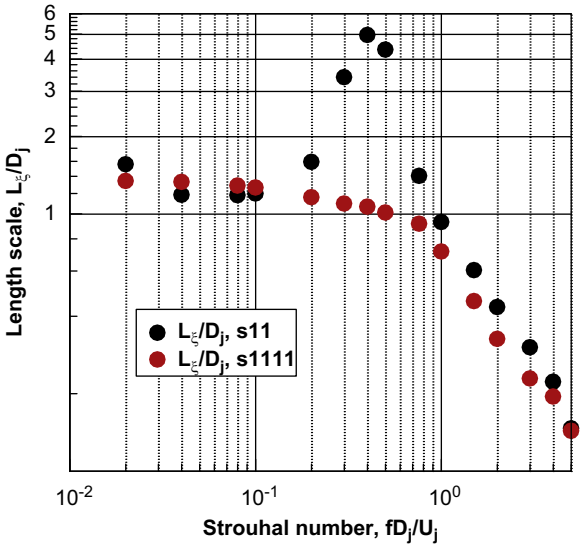

Fig. 25. Variation of axial, radial and azimuthal length scales with Strouhal number: $x/D_j = 5$ and $r/D_j = 0.0$.

coincidentally, the present measurements on the jet lip line give values that are the square of the LES results. The present results were obtained from both averages of the velocity data as well as from the cross correlation functions. A possible cause of the discrepancy could be the effect of the very small separation in the cross wire locations. It is readily shown, for example, that the turbulence intensities and shear stress, as well as the higher order statistics, calculated from the cross wire depend on the correlation of the velocity fluctuations between the two wires. In the present experiments, the wire separation was approximately 0.076 cm or $0.015D_j$. Based on the two wire measurements, the correlation can vary slightly over this small distance.

4. Comparison with RANS simulations

Predictions of the average flow development have been made using the NPARC Wind-US 2.0 code. Fig. 29 shows a comparison of the predicted centerline velocity with the experiments. It is clear that the RANS calculation over-predicts the length of the potential core and the subsequent rate of decay of the jet centerline velocity. Fig. 30 shows the relative values on the jet centerline of the turbulent kinetic energy to its maximum compared to the experimental measurements.

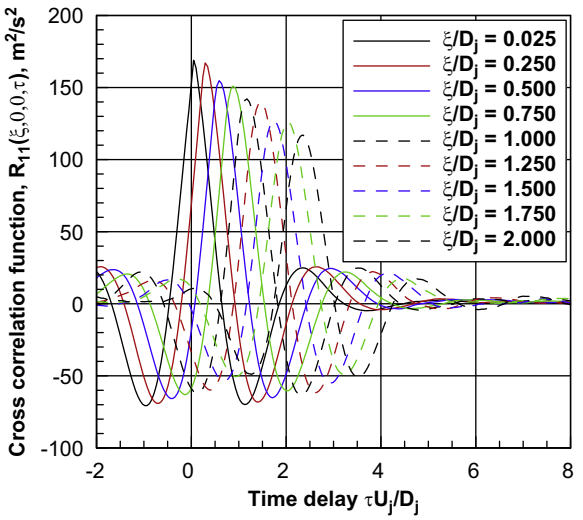

Fig. 26. Cross correlation function for axial velocity fluctuations: $x/D_j = 5$ and $r/D_j = 0.0$.

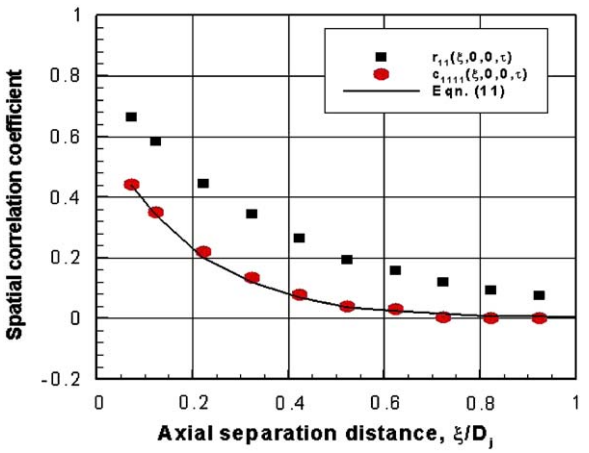

Fig. 27. Spatial cross correlation coefficients: $x/D_j = 9$ and $r/D_j = 0.0$.

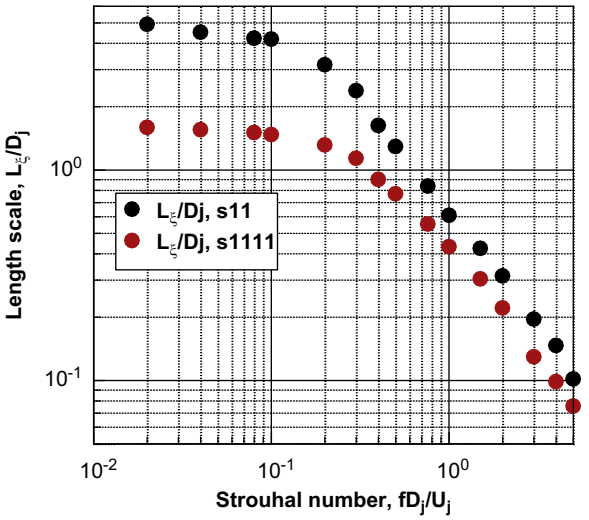

Fig. 28. Variation of axial length scales with Strouhal number: $x/D_j = 9$ and $r/D_j = 0.0$.

Table 2
Values of the fourth order autocorrelation functions relative to C_{1111} at different locations in the jet.

x/D_j	r/D_j	C_{2222}	C_{1212}	C_{1122}
1.5	0.5	0.13	0.21	0.06
5.0	0.5	0.16	0.23	0.05
9.0	0.5	0.18	0.23	0.05
5.0	0.0	0.85	0.46	0.16
6.0	0.0	0.42	0.33	0.18
7.0	0.0	0.31	0.30	0.13
8.0	0.0	0.32	0.32	0.09
9.0	0.0	0.31	0.31	0.05

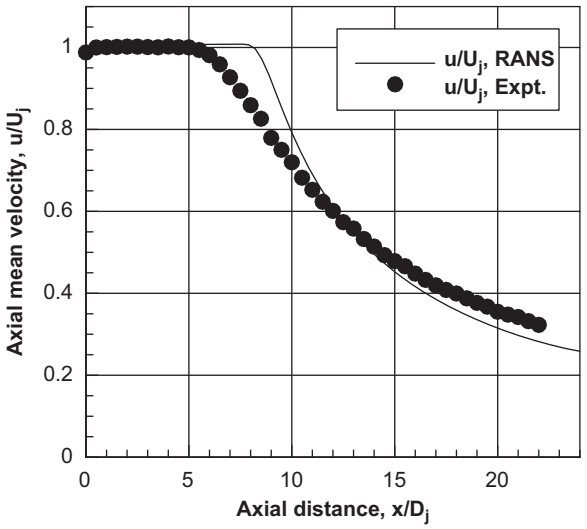

Fig. 29. Comparison of RANS simulations and experimental measurements of axial mean velocity on the jet centerline.

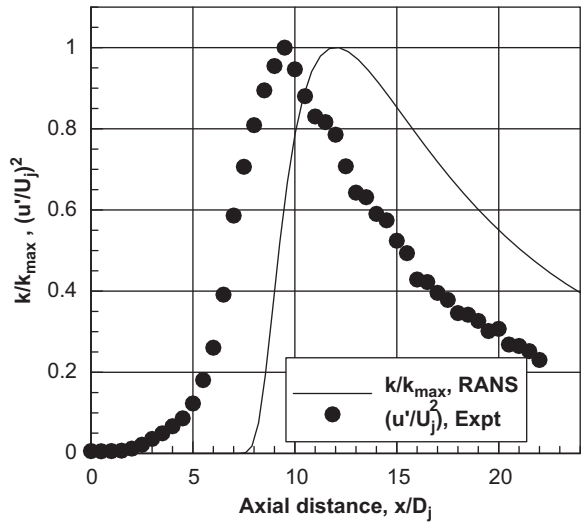

Fig. 30. Comparison of RANS simulations and experimental measurements of turbulent kinetic energy and mean square axial velocity fluctuations on the jet centerline.

The predictions give a peak location at $x/D_j = 12$, whereas the experiments give a peak at $x/D_j = 9$. However, the turbulence model coefficients have been optimized for boundary layer flows and it well known that these values underpredict the mixing rate: see Thies and Tam [26] and Barber et al. [27]. However, here the aim is to compare the

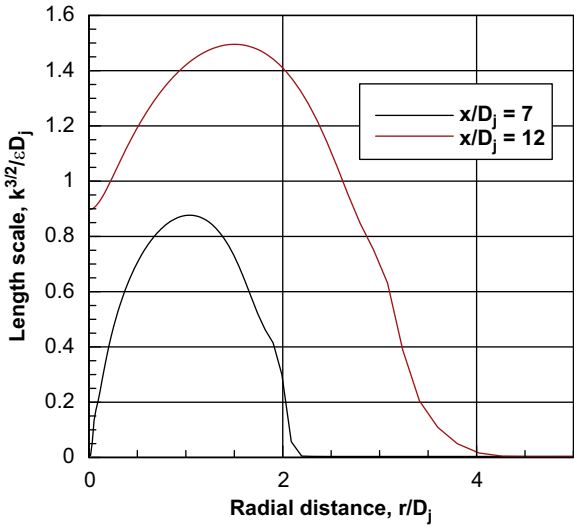

Fig. 31. Predicted radial variation of length scale $k^{3/2}/(\varepsilon D_j)$ from RANS simulations.

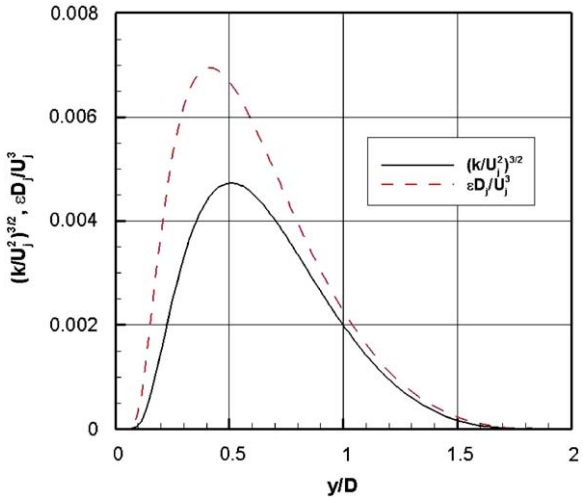

Fig. 32. Predicted radial variation of turbulent kinetic energy, shown as $(k/U_j^2)^{3/2}$), and viscous dissipation rate $\varepsilon D_j/U_j^3$ at $x/D_j = 7$.

measured length scales with those estimated from the RANS simulations. So, the measured values at 5 and 9 diameters are compared with the simulated values at 7 and 12 diameters. Fig. 31 shows the variation of the length scale based on the predicted turbulent kinetic energy and viscous dissipation rate at these two axial locations. The length scale in the simulations is defined by $k^{3/2}/\varepsilon$. There are several interesting features of these plots. The maximum predicted length scale occurs at more than twice the jet radius. The reason for this can be seen in Fig. 32. The turbulent kinetic energy and the viscous dissipation rate both have maxima near the jet lip line. However, the ratio $k^{3/2}/(\varepsilon D_j)$ peaks much further from the jet centerline. This is well away from the maximum values of k and ε. However, the relevant value of length scale for noise prediction purposes should be the value close to the lip line. This would be approximately $0.7D_j$ and $1.2D_j$ at $x/D_j = 7$ and $x/D_j = 12$, respectively. The measured axial length scales based on the $1/e$ values, as given in the previous sections, are much lower than this. For example, the axial length scales based on the second order spatial correlations are $0.295D_j$ and $0.403D_j$ at $x/D_j = 5$ and $x/D_j = 9$, respectively. These are the measured values on the jet lip line. It is encouraging that the ratio of the length scales is 1.7 and 1.4 for the simulated and measured scales, respectively. The length scales associated with the lower Strouhal numbers, shown in Figs. 15 and 17 are much larger than the predicted values for the second order correlations, being approximately $2.5D_j$ and $4.0D_j$ at $x/D_j = 5$ and $x/D_j = 9$, respectively. However, the length scales based on the fourth order correlations are very similar to the simulated values being approximately $1.0D_j$ and $1.5D_j$ at $x/D_j = 5$ and $x/D_j = 9$, respectively. Though this is probably coincidental, the comparisons in this section could be argued to justify

the use of RANS simulations for estimating the length scales of both the fine scale turbulence as well as the properties of the large scale turbulent structures. Clearly, a different coefficient would be required in the two cases and this would only apply to regions of high turbulence intensity, not to locations inside or near the jet potential core. It could also be argued that the use of a length scale based purely on the axial distance or the local shear layer width would be adequate. However, that would not be the case for multi-stream or non-circular jets.

5. Summary and conclusions

This paper has described measurements of the statistical properties of turbulent velocity fluctuations in a subsonic jet. Both second and fourth order two point statistics of the axial velocity fluctuations and single point statistics of the axial and radial velocity fluctuations have been measured. The length scales based on the overall spatial correlations as well as the variation of the length scales with Strouhal number have been determined at different locations in the jet: primarily on the jet center and lip lines. The characteristics of the statistical properties are very similar in the regions of highest turbulent velocity fluctuations. This is encouraging for statistical models used in noise source modeling that generally are assumed to have similar forms at all locations in the jet. The regions where there are distinct differences are close to the edge of the jet potential core. However, these are not regions of high turbulence intensity. The flatness factor for the axial velocity fluctuations has also been measured throughout the jet. Again, in regions of high turbulence intensity its value is quite uniform, being slightly less than the value of three for a normal distribution. This provides some justification for the use of the quasi-normal hypothesis in noise source modeling. However, it has been shown that the fourth and second order statistical properties of the axial velocity fluctuations in the jet are related without any assumptions regarding the nature of the statistical process. This provides justification for noise source models that depend on the fluctuations in the second order properties rather than the fluctuations themselves. For noise models where the equivalent source terms are already second order or higher in the fluctuations, such as models based on Lilley's equation or the linearized Euler equations, this would simply mean always subtracting the average of the model equations. This has been done, for example, in Goldstein's model [20].

Comparisons between RANS simulation of the flow and the measurements have provided some encouragement that the evaluation of length scales based on the simulations can be used in the scaling of the models. It is probable that a length scale based on the axial distance or local width of the jet shear layer would work just as well—at least for single stream axisymmetric jets. However, it has been shown that there is a significant variation in length scale with Strouhal number. Any noise prediction model that aims at capturing the physics of the noise generation process, rather than simply making noise predictions, should take this variation into account. Though, it could be argued that the nearly constant length scale at lower Strouhal numbers is more an indication of the properties of the large scale structures in the turbulence and shouldn't play a role in the prediction of noise from fine scale turbulence.

Though hot-wire measurements do suffer from limitations, both in terms of probe interference effects as well as in the flow velocities that can be considered, the results in the present paper demonstrate that much can be learned from them. It is hoped that additional measurements with multiple cross wire probes will be conducted in the future in order to extend the data base described in the present paper.

Acknowledgments

These experiments were conducted while P.J. Morris was on sabbatical leave at the NASA Glenn Research Center. He appreciates the hospitality shown to him by the Aeropropulsion Division, particularly the Acoustics and Inlet & Nozzle Branches. The Wind-US simulations were performed by Mr. Steven Miller of the Department of Aerospace Engineering at Penn State University. This research was sponsored under a NASA Cooperative Agreement NNX07AC88A entitled, A Comprehensive Model for the Prediction of Supersonic Jet Noise. The Technical Monitor is Dr. Milo Dahl.

References

[1] P.O.A.L. Davies, M.J. Fisher, M.J. Barratt, The characteristics of turbulence in the mixing region of a round jet, *Journal of Fluid Mechanics* 15 (1963) 337–367.
[2] P. Bradshaw, D.H. Ferriss, R.F. Johnson, Turbulence in the noise-producing region of a circular jet, *Journal of Fluid Mechanics* 19 (1964) 591–624.
[3] P.O.A.L. Davies, Turbulence structure in free shear layers, *AIAA Journal* 4 (11) (1966) 1971–1978.
[4] W.T. Chu, Turbulence Measurements Relevant to Jet Noise, UTIAS Report 119, University of Toronto, Toronto, Canada, November 1966.
[5] A. Michalke, H.V. Fuchs, On turbulence and noise of an axisymmetric shear flow, *Journal of Fluid Mechanics* 70 (1) (1975) 179–205.
[6] M. Harper-Bourne, Jet near-field noise prediction, AIAA Paper 1999-3214, 1999.
[7] M. Harper-Bourne, Jet noise turbulence measurements, AIAA Paper 2003-3214, 2003.
[8] C.K.W. Tam, L. Auriault, Jet noise from fine-scale turbulence, *AIAA Journal* 37 (2) (1999) 145–153.
[9] P.J. Morris, S. Boluriaan, The prediction of noise from CFD data, AIAA Paper 2004-2977, 2004.
[10] J. Bridges, M. Wernet, Effect of heat on space–time correlations in jets, AIAA Paper 2006-2534, 2006.
[11] M.P. Wernet, Temporally resolved PIV for space–time correlations in both cold and hot jet flows, *Measurement Science and Technology* 18 (2007) 1387–1403.
[12] F. Kerhervé, P. Jordan, Y. Gervais, J.-C. Valière, P. Braud, Two-point laser Doppler velocimetry measurements in a Mach 1.2 cold supersonic jet for statistical aeroacoustic source model, *Experiments in Fluids* 37 (2004) 419–437.

[13] F. Kerhervé, J. Fitzpatrick, P. Jordan, The frequency dependence of jet turbulence for noise source modeling, *Journal of Sound and Vibration* 296 (2006) 209–225.
[14] F. Kerhervé, J. Fitzpatrick, Modelling the frequency dependence of two-point turbulence properties in jet flows, AIAA Paper 2007-3665, 2007.
[15] L. Chatellier, J. Fitzpatrick, Spatio-temporal correlation analysis of turbulent flows using global and single-point measurements, *Experiments in Fluids* 38 (2005) 563–575.
[16] L. Ukeiley, C.E. Tinney, R. Mann, M. Glauser, Spatial correlations in a transonic jet, *AIAA Journal* 45 (6) (2007) 1357–1369.
[17] V. Fleury, C. Bailly, E. Jondeau, M. Michard, D. Juvé, Space–time correlations in two subsonic jets using dual particle image velocimetry measurements, *AIAA Journal* 46 (10) (2008) 2498–2509.
[18] M.J. Doty, D.K. McLaughlin, Space–time correlation measurements of high-speed axisymmetric jets using optical deflectometry, *Experiments in Fluids* 38 (4) (2005) 415–425.
[19] A. Khavaran, J. Bridges, Modelling of fine-scale turbulence mixing noise, *Journal of Sound and Vibration* 279 (2005) 1131–1154.
[20] M.E. Goldstein, A generalized acoustic analogy, *Journal of Fluid Mechanics* 488 (2003) 315–333.
[21] S.A. Karabasov, M.Z. Afsar, A.P. Hynes, T.P. Dowling, W.A. McMullan, C.D. Pokora, G.J. Page, J.J. McGuirk, Using large eddy simulation with an acoustic analogy approach for jet noise modelling, AIAA Paper 2008-2985, 2008.
[22] G.K. Batchelor, *The Theory of Homogeneous Turbulence*, Cambridge University Press, Cambridge, MA, 1953.
[23] M.J. Lighthill, An estimate of the covariance without using statistical assumptions. Appendix 1 of "On the noise radiated from a turbulent high speed jet," by G.M. Lilley, in: J.C. Hardin, M.K. Hussaini (Eds.), *Computational Aeroacoustics*, Springer, New York, 1993, pp. 112–113.
[24] M.J. Fisher, P.O.A.L. Davies, Correlation measurement in a non-frozen pattern of turbulence, *Journal of Fluid Mechanics* 18 (1) (1964) 97–116.
[25] R.H. Self, Jet noise predictions using the Lighthill acoustic analogy, *Journal of Sound and Vibration* 275 (2004) 757–768.
[26] A.T. Thies, C.K.W. Tam, Computation of turbulent axisymmetric and nonaxisymmetric jet flows using the K-epsilon model, *AIAA Journal* 34 (2) (1996) 309–316.
[27] T.J. Barber, L.M. Chiappetta, J.R. DeBonis, N.J. Georgiadis, D.A. Yoder, Assessment of parameters influencing the prediction of shear-layer mixing, *Journal of Propulsion and Power* 15 (1) (1999) 45–53.